

# Rapid motion correction in MR-guided high-intensity focused ultrasound heating using real-time ultrasound echo information

Philippe Lourenço de Oliveira, Baudouin Denis de Senneville, Iulius Dragonu, Chrit Moonen

## ► To cite this version:

Philippe Lourenço de Oliveira, Baudouin Denis de Senneville, Iulius Dragonu, Chrit Moonen. Rapid motion correction in MR-guided high-intensity focused ultrasound heating using real-time ultrasound echo information. *NMR in Biomedicine*, Wiley, 2010, 23 (9), pp.1103-1108. <10.1002/nbm.1526>. <hal-01503908>

**HAL Id: hal-01503908**

**<https://hal.archives-ouvertes.fr/hal-01503908>**

Submitted on 7 Apr 2017

**HAL** is a multi-disciplinary open access archive for the deposit and dissemination of scientific research documents, whether they are published or not. The documents may come from teaching and research institutions in France or abroad, or from public or private research centers.

L'archive ouverte pluridisciplinaire **HAL**, est destinée au dépôt et à la diffusion de documents scientifiques de niveau recherche, publiés ou non, émanant des établissements d'enseignement et de recherche français ou étrangers, des laboratoires publics ou privés.

# Rapid<sup>Q1</sup> motion correction in MR-guided high-intensity focused ultrasound heating using real-time ultrasound echo information

Philippe Lourenço de Oliveira<sup>a</sup>, Baudouin Denis de Senneville<sup>a\*</sup>, Iulius Dragonu<sup>a</sup> and Chrit T. W. Moonen<sup>a</sup>

The objective of this study was to evaluate the feasibility of integrating real-time ultrasound echo guidance in MR-guided high-intensity focused ultrasound (HIFU) heating of mobile targets in order to reduce latency between displacement analysis and HIFU treatment. Experiments on a moving phantom were carried out with MRI-guided HIFU during continuous one-dimensional ultrasound echo detection using separate HIFU and ultrasound imaging transducers. Excellent correspondence was found between MR- and ultrasound-detected displacements. Real-time ultrasound echo-based target tracking during MR-guided HIFU heating is shown with the dimensions of the heated area similar to those obtained for a static target. This work demonstrates that the combination of the two modalities opens up perspectives for motion correction in MRI-guided HIFU with negligible latency. R1.8 Copyright © 2010 John Wiley & Sons, Ltd.

**Keywords:** motion correction; real time; MRI; ultrasound echo

## INTRODUCTION

High-intensity focused ultrasound (HIFU) is a promising non-invasive technique for the local deposition of thermal energy deep inside the human body (1,2). MRI guidance of this method offers the benefits of excellent target visualisation and continuous temperature mapping using the proton resonance frequency (PRF) shift technique (3).

For the ablation of tumours in abdominal organs by MR-controlled HIFU under free breathing, the current target position must be continuously tracked in order to reposition the HIFU focal point to avoid undesirable damage of nearby healthy tissue.

It has been demonstrated that a HIFU system based on a phased-array ultrasound (US) transducer and rapid electronic displacement of the focal point, in combination with advanced real-time processing of MR images with correction of motion artefacts in temperature mapping, allows a mobile target to be tracked during the heating procedure, and enables regional temperature control (4,5). Complex deformations can be estimated and the technique enables the correction of the focal point position for periodical complex motions (rigid or elastic). However, the main difficulty is that the time duration between actual target displacement and MR-derived motion information is not negligible. This delay is the sum of a part of the acquisition time, the reconstruction time, the data transfer and the treatment planning (processing k-space data, Fourier transformation, thermal map computation, motion estimation, modelling of energy absorption and heat conduction via the bio heat transfer equation). A fast imaging update time is required, but this limits the spatial and/or temporal resolution, volume coverage and temperature precision of the scanned volume. For these reasons, the periodical motion should be anticipated to allow accurate

HIFU positioning. This anticipation process imposes a high reproducibility of the motion with small modifications of the period duration and amplitude. For most therapeutic applications within the human body, tissue displacement is usually caused by the respiratory and/or cardiac cycle, and can be assumed to be periodic in anaesthetised patients. However, this may not be the case for free-breathing patients. In this context, two approaches are currently being investigated in our laboratory.

1. To provide a computationally effective processing pipeline for MR temperature maps in conjunction with high-frame-rate imaging to achieve a subsecond temporal resolution.
2. To use external sensors to provide independent motion information with high temporal resolution that can be employed, in conjunction with MR images, to estimate the target position.

\* Correspondence to: B. D. de Senneville, UMR 5231, Imagerie Moléculaire et Fonctionnelle, Université 'Victor Segalen' Bordeaux 2, 146, rue Léo Saignat, case 117, 33076 Bordeaux, France.  
E-mail: baudouin@imf.u-bordeaux2.fr

a P. L. de Oliveira, B. D. de Senneville, I. Dragonu, C. T. W. Moonen  
Laboratory for Molecular and Functional Imaging: From Physiology to Therapy, UMR 5231 CNRS/Université Bordeaux 2, Bordeaux, France

Contract/grant sponsors: Ligue Nationale Contre le Cancer, Conseil Régional d'Aquitaine; Diagnostic Molecular Imaging EC-FP6-project LSHB-CT-2005-512146; Agence National de la Recherche; project MRgHIFU-ALKT.; Phillips [Healthcare](#)<sup>Q3</sup>.

**Abbreviations used used:** ADC, analogue to digital converter; EPI, echo planar imaging; FWHM, full width at half-maximum; HIFU, high-intensity focused ultrasound; MSPS, mega samples per second; PRF, proton resonance frequency; RF, radiofrequency; RMS, root mean square; SSFP, steady state free precession; US, ultrasound.

The aim of this study is to investigate the feasibility of the latter, using additional motion information provided by a US tracking system. US has been demonstrated to be a powerful tool for the evaluation of target displacement estimation (6). It has been shown in phantoms that US imaging can be used to correct, a posteriori, steady state free precession (SSFP)-type rapid MR images (7). In this communication, it is demonstrated in a phantom study that MR- and US-based estimated displacements are identical, and that a simple one-dimensional US echo can be used in combination with real-time volumetric MRI thermometry. For real-time purposes, it is shown that echo information is processed and results rapidly transferred to correct MR temperature maps, as well as to adapt HIFU focal point position and intensity.

## MATERIALS AND METHODS

In order to demonstrate the feasibility of using, in real time, US echo information to improve real-time MR temperature monitoring of mobile targets, the following studies were carried out.

1. The analysis of the correlation of on-line MR- and US-based displacement estimation during periodic motion of a phantom using short data processing times compatible with on-line performance.
2. The analysis of the precision of HIFU heating with direct US-based tracking of a mobile target in real time, together with simultaneous volumetric MRI thermometry, without displacement anticipation, in comparison with heating of the immobilised target.

### Evaluation platform

Figure 1 shows details of the experimental platform.

#### MR acquisition

Dynamic MR temperature imaging was performed on a [Philips<sup>O4</sup>](#) Achieva 1.5 Tesla with a single-shot, gradient-recalled, echo planar imaging (EPI) sequence with a surface coil (diameter,

12 cm) placed around the target. Real and imaginary data were transferred online to a computer for temperature visualisation and control of the HIFU driver for repositioning of the heating point. This computer was equipped with a Centrino Duo 2GHz processor and 2 GB of RAM running under the Windows XP operating system.

#### HIFU system

An inhouse-built, 256-channel, focused phased array transducer, operating at 1.5 MHz and with a focal length of 80 mm, was used to steer the focal point electronically. The positioning of the 256 individual elements (5.8 mm in diameter) was optimised for minimal intensity of secondary lobes and compactness of the transducer (8). For this purpose, an iterative optimisation scheme, according to an acoustic field simulation based on Rayleigh integration, was performed to design the transducer. A conventional LC impedance matching was adjusted for each electrical impedance of the 256 channels to transform a typical complex impedance of 20–280 J into 50 Ω. The power and position of the focal point could be updated electronically every 65 ms. During hyperthermia, 100 W of electric energy were transmitted in a focal dimension at -6 dB of 1 × 1 × 5 mm<sup>3</sup> with a maximal pressure of 6.1 MPa.

#### US motion estimation system

A single-channel pulse/receiver filtered against MR frequency (USBx, [Lecoeur<sup>O5</sup>](#)-Electronique, France) was connected to a single transducer element (outside diameter, 6 mm; identical to the components of the 256-element phased array system described above), operating at 1.2 MHz with a beam profile [characterised<sup>O6</sup>](#) by 13.5° and an aperture angle of -6 dB, to evaluate the one-dimensional target displacement along the transducer direction. The received signal amplitude is about -40 [dBm<sup>O7</sup>](#). Each 20 ms (limited by the USB driver communication used), a radiofrequency (RF) pulse was emitted and processed for motion estimation. An analogue to digital converter (ADC) of 10 bits was used, operating at 20 megasamples per second (MSPS). The sensitive region of the US tracking probe was centred on the mean position of the water-gel interface.

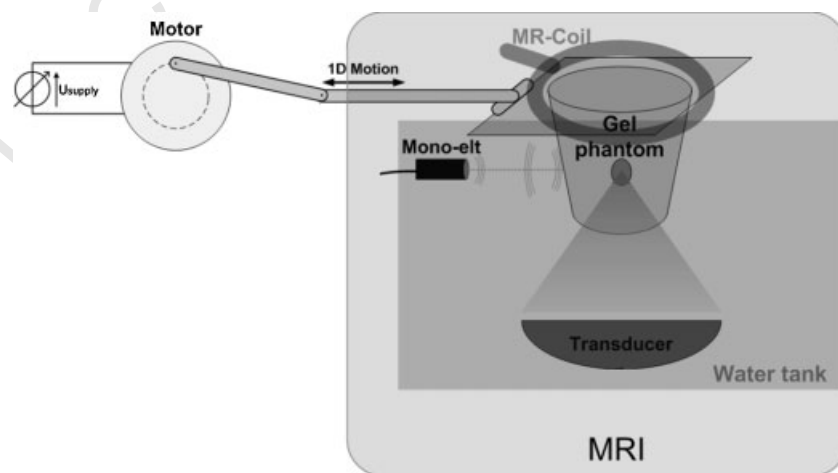


**Figure 1.** Experimental platform designed to evaluate the feasibility of correlating MR- and ultrasound (US)-based motion estimations, and of real-time ultrasound tracking of a mobile target with simultaneous real-time volumetric MRI thermometry. The single-element ultrasound imaging transducer is indicated as 'Mono-elt'. 1D, one-dimensional.

61  
62  
63  
64  
65  
66  
67  
68  
69  
70  
71  
72  
73  
74  
75  
76  
77  
78  
79  
80  
81  
82  
83  
84  
85  
86  
87  
88  
89  
90  
91  
92  
93  
94  
95  
96  
97  
98  
99  
100  
101  
102  
103  
104  
105  
106  
107  
108  
109  
110  
111  
112  
113  
114  
115  
116  
117  
118  
119  
120

1 *Physiological phantom*

2 A gel phantom (diameter, 10 cm), composed of agar, silica and  
3 water with relaxation times matched to the human kidney, and a  
4 US attenuation close to that of abdominal organs (approximately  
5 1 dB/cm at 1.2 MHz), was mounted on a motorised platform to  
6 simulate an abdominal organ. Its displacement was remotely  
7 controlled by a mechanical transmission line. The motorised  
8 phantom performed a periodic sinusoidal one-dimensional  
9 displacement. The motion period was varied by adjusting the  
10 voltage supply applied to the motor. The displacement direction  
11 was parallel to the tracking mono-element axis, allowing a direct  
12 displacement evaluation.

13 **Correlation of online MR- and US-based motion estimations**

14 *MR imaging*

15 Single-slice MR images with a resolution of  $96 \times 96$  pixels and a  
16 pixel size of  $1.55 \times 1.55 \times 1.55 \text{ mm}^3$  were obtained every 300 ms  
17 (TE = 27 ms) during a periodic motion of the phantom with a  
18 maximum amplitude of 30 mm. During 55 s, several motion cycles  
19 with different period durations (between 0 and 0.73 Hz) were  
20 applied successively, with the target finally returning to its  
21 original position. Simultaneously, US echoes were recorded.

22 *MR motion estimation*

23 Image processing techniques can be used to estimate online  
24 organ displacements from anatomical images (9,10). Image  
25 registration allows a robust estimation of organ displacement  
26 with excellent two-dimensional/three-dimensional spatial infor-  
27 mation (11) when compared with other existing approaches,  
28 such as those using MR navigator signals (12) or US echoes (6,7).  
29 The objective is to relate the coordinate of each part of tissue  
30 in the image to register with the corresponding part in a  
31 reference image (typically the first of the temporal series). In  
32 this communication, the translational transformation was est-  
33 imated using a differential approach of Gauss–Newton (13).  
34 MR-based estimated displacements were compared with gold  
35 standard positions available from the motion platform in (4), and  
36 demonstrated to be accurate with a precision better than 1/4  
37 pixel. Positions available from the motion platform are therefore  
38 not reported in this study.

39 *US motion estimation*

40 The motion was estimated using a speckle tracking technique: a  
41 one-dimensional cross-correlation algorithm (14,15) between a  
42 reference and the current RF signal was used to estimate the  
43 time-shift corresponding to the target displacement along the  
44 beam axis of the mono-element.

45 *Real-time synchronisation of MR- and US-based motion estimations*

46 A temporal synchronisation of MR- and US-based motion  
47 estimations is required. For this purpose, an oscilloscope kept  
48 track of the start of the MR pulse sequence with a microsecond  
49 temporal resolution, and this information was transferred to the  
50 computer (see Fig. 1). Two constant delays were then taken into  
51 account for comparison: (i) a delay related to MRI (similar to the  
52 aperture time for a snapshot with a camera) which corresponds  
53 to half the image acquisition time (equal to TE in the case of a

single-shot, gradient-echo, EPI sequence); (ii) a delay related to  
the US system, which relates to the time duration in US echoes  
(less than a millisecond).

61 *Assessment of correlation between MR- and US-based motion estimation*

62 The correlation between MR- and US-based motion estimation  
63 was analysed using a linear regression, considering a significant  
64 Pearson correlation ( $R^2$ ) higher than 0.95. The slope and  
65 y-intercept values were compared with the identity function.  
66 The residual fitting error was evaluated with an average absolute  
67 mean difference. In addition, the root mean square (RMS) value  
68 between MR- and US-based motion estimations was evaluated  
69 for different motion period durations.

70 **Real-time US tracking of a mobile target with simultaneous real-time volumetric MRI thermometry**

71 *MR imaging*

72 The amplitude of the periodical phantom (period, 6 s) motion was  
73 set to 10 mm along the z-axis. The phantom was heated with  
74 HIFU using 100 W of acoustic power during 20 s. MR volumetric  
75 thermometry data were obtained using three slices with a  
76 resolution of  $96 \times 96$  pixels and a pixel size of  $1.33 \times 1.33 \times$   
77  $6 \text{ mm}^3$  every 360 ms (TE, 46 ms).

78 *HIFU positioning with motion*

79 US-based estimated motion was used to adjust the focal point of  
80 the HIFU device to the current location of the chosen target.  
81 However, US-based motion estimation and HIFU sonication  
82 cannot operate simultaneously because of the proximity of the  
83 operating frequencies of the two devices, and the high HIFU  
84 power amplitude with regard to the receiver signal amplitude  
85 used for US tracking. For this reason, temporal multiplexing was  
86 necessary: the HIFU generator was successively ON during 65 ms  
87 and OFF during 25 ms, allowing US motion estimation system  
88 from speckle acquisition. Therefore, the HIFU sonication was  
89 updated every 90 ms.

90 *Online MR temperature monitoring of the mobile target*

91 Motion-compensated MR thermometry was performed as  
92 presented in (4,16). This PRF-based method acquires a  
93 complete set of reference magnitude and phase images for  
94 each organ position during a pretreatment step. During the  
95 intervention, the current magnitude image was compared with  
96 the prerecorded set and the closest match was selected by  
97 evaluating the intercorrelation coefficient. The corresponding  
98 prerecorded phase image served as reference for current  
99 temperature computation. This strategy allows the correction  
100 of online periodical interscan motion-related errors in PRF  
101 temperature methods.

102 **RESULTS**

103 **Comparison between MR- and US-based motion estimations**

104 The implemented image registration algorithm required 50 ms of  
105 computation time on our HIFU computer for one image with a  
106 resolution of  $96 \times 96$  pixels, and is thus compatible with online  
107 conditions. Figure 2 compares online MR- (in red) and US- (in

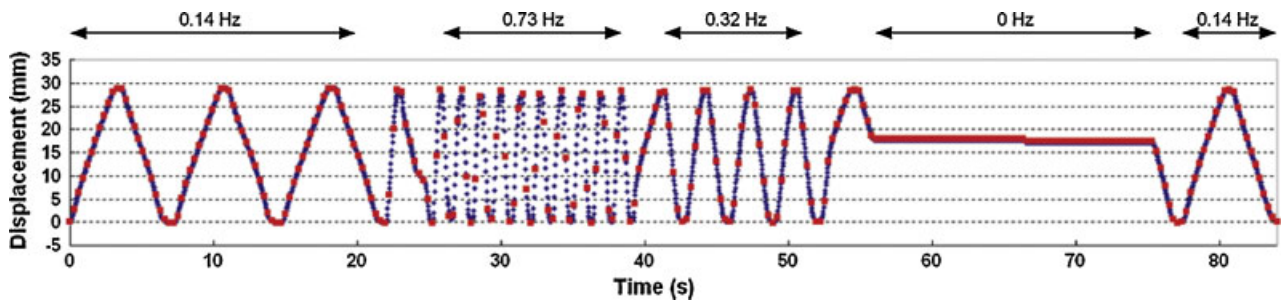


**Figure 2.** Comparison between MR- (in red) and ultrasound (US)- (in blue) based displacement estimations obtained for a phantom undergoing different periodic motion with varying frequencies.

blue) based estimated displacements. A linear regression resulted in an identity function (the slope and  $y$ -intercept values are 1.01 and 0.04, respectively) with an excellent correlation ( $R^2 = 0.9991$ ), as shown in Fig. 3a. The average absolute error between MR- and US-based displacement estimations was approximately equal to 0.22 mm (maximum, 1.39 mm). Figure 3b reports the RMS value of the difference between MR- and US-based displacement estimations for different target motion frequencies. It can be observed that this RMS value increases linearly with the motion frequency.

#### Direct US tracking of a mobile target with simultaneous real-time volumetric MRI thermometry

Figure 4 shows the spatial temperature distribution obtained with an immobilised target (Fig. 4a), and with a target undergoing a periodical translation without (Fig. 4b) and with (Fig. 4c) adjustment of the focal point position, after 15 s of heating. The results obtained on the immobilised target are used as a gold standard for comparison: a maximal temperature increase of  $19.5^\circ\text{C}$  was measured and the full width at half-maximum (FWHM) area dimensions were  $4.3 \times 4.2 \text{ mm}^2$ . Without focal point position correction (Fig. 4b), the heated area extended over a length of 12 mm (heating area dimensions,  $4 \times 12 \text{ mm}^2$ ) and only a  $10.2^\circ\text{C}$  maximum temperature increase was obtained. With focal repositioning based on US echo (Fig. 4c), the heated area

had a circular shape and the energy was deposited over the same tissue area relative to that for the immobilised phantom. The heating area dimensions were  $4.3 \times 4.5 \text{ mm}^2$  and a maximum temperature increase of  $16.3^\circ\text{C}$  was measured.

## DISCUSSION

### Correlation of online MR- and US-based displacement estimations

It can be observed from Figs 2 and 3 that the displacement estimated with each modality matches precisely for different motion frequencies. The uncertainty of the reported results depends on the robustness of the motion estimation method relative to each modality, the accuracy of the synchronisation technique and the evaluation platform. Figure 3b shows that there is a small discrepancy between US- and MRI-derived displacements depending on the frequency of the periodic motion. Intrascan motion artefacts may hamper motion estimation based on MR images, especially in the case of rapid target displacement. Intrascan motion artefacts were minimised using a fast single-shot EPI sequence. In addition, some uncertainty may be related to geometric distortions in MR images. Although the MR sequences have been optimised to avoid geometrical distortions in our study, appropriate real-time corrections (17) may be applied in regions prone to high susceptibility changes

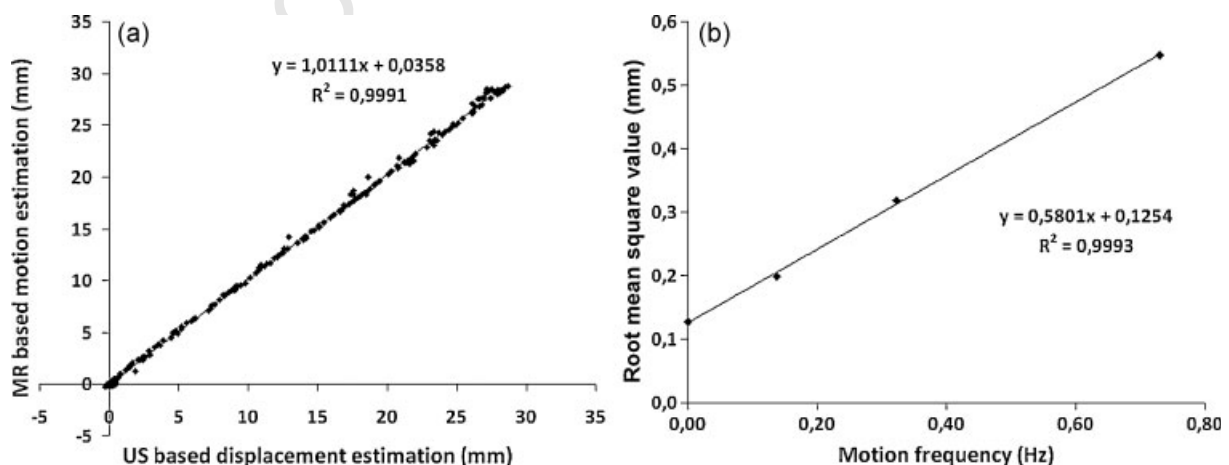


**Figure 3.** Quantitative evaluation of the correlation between MR- and ultrasound (US)-based displacement estimations: (a) relationship between MR- and US-based displacement estimations reported in Fig. 2 for each dynamic MR acquisition; (b) evaluation of the root mean square (RMS) value between MR- and US-based displacement estimations for different motion frequencies.

61  
62  
63  
64  
65  
66  
67  
68  
69  
70  
71  
72  
73  
74  
75  
76  
77  
78  
79  
80  
81  
82  
83  
84  
85  
86  
87  
88  
89  
90  
91  
92  
93  
94  
95  
96  
97  
98  
99  
100  
101  
102  
103  
104  
105  
106  
107  
108  
109  
110  
111  
112  
113  
114  
115  
116  
117  
118  
119  
120

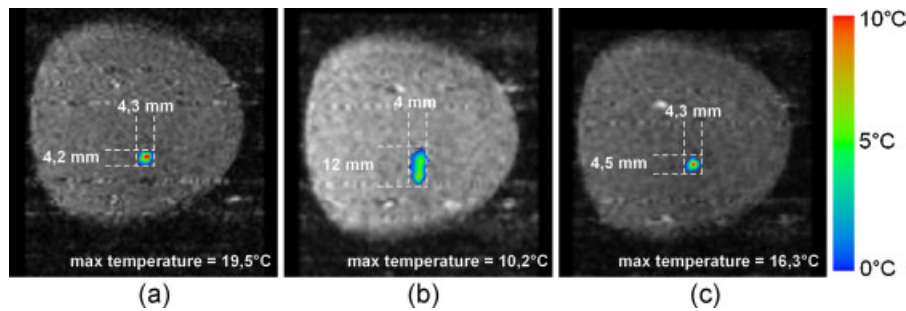


**Figure 4.** Temperature difference maps obtained online after 15 s of heating with an immobilised target (a), and with a target undergoing a periodical motion without (b) and with (c) the focal point position corrected in real time based on ultrasound echo information.

(especially near tissue–air and tissue–bone interfaces). Although a maximal difference between the two estimated positions of 1.39 mm was observed for extreme target positions at the highest motion frequency (0.73 Hz), a very good correspondence between MR- and US-based displacement estimations was always obtained.

### Real-time US tracking of a mobile target with simultaneous volumetric MRI thermometry

US echo-based target tracking of a single heated point allowed a controlled temperature increase comparable with that in the reference experiment on the static phantom. The size of the heated region size was similar for the moving phantom relative to that of the stationary phantom, indicating accurate HIFU tracking. The time lag of the HIFU sonication was limited by both US acquisition and processing (equivalent to the US signal acquisition + data transfer + processing time, and equal to 20 ms in our study) and by the lag time to update the HIFU system (90 ms in our study). Although the hardware should still be optimised further in the case of fast target displacement, it was sufficient in this study (mimicking respiratory related displacements of the liver and kidney) to demonstrate the feasibility of the tracking studies. However, the maximal temperature increase with the tracked experiment was somewhat lower than the reference experiment on the immobilised target (16.3°C compared with 19.5°C, respectively). Two hypotheses may explain this decrease in temperature. First, the observed decrease in temperature may arise from partial volume effects in MRI thermometry. Second, the observed decrease may also arise from the laterally focused beam as a result of the transducer element directivity (lower energy deposition in the targeted area when the focal point moves out of the geometric focus as a result of secondary lobes).

The excellent temporal resolution of the displacement information update allowed tracking of the mobile target with negligible latency. Therefore, no anticipation process is required, avoiding restrictions with regard to target displacement (periodicity of the motion, accidental motions). The results obtained demonstrate the feasibility of continuous HIFU treatment in an *ex vivo* moving phantom with a frequency of approximately that of the respiratory cycle. It was also demonstrated that this fast US tracking can be performed simultaneously with quantitative volumetric MRI thermometry.

## CONCLUSION

Although it is well established that MR imaging can provide motion estimates with a high spatial resolution, it is difficult in

practice to acquire online three-dimensional isotropic images because of technical limitations, spatial and temporal resolution trade-offs, and low SNR associated with fast three-dimensional acquisition sequences. In addition, the time duration between the actual target displacement and the availability of the motion information from MR data is not negligible. Therefore, an anticipation process is required, imposing restrictions on the motions that can be corrected for. This study demonstrates the excellent correlation of MR- and US-based displacement estimation. In addition, US echo information has been shown to give a fast continuous update of displacement information, allowing real-time tracking of a mobile target with negligible latency, and thus avoiding the requirement of any anticipation in the HIFU firing pattern. Although the hardware should still be optimised further (as the HIFU sonication update rate is limited by the 90 ms lag to update the HIFU generator), it was sufficient to demonstrate the principle of the feasibility study. This study opens up perspectives to combine MR and US modalities to provide accurate spatial and temporal estimation of target displacement together with online MR temperature monitoring.

This feasibility study was performed with simplified one-dimensional US tracking and two-dimensional MR imaging with unidirectional displacements. In order to apply such methods *in vivo*, further improvements will be required, as, in this case, the target may move in oblique angles with respect to the US probe. The results obtained in this communication suggest two paths of investigation. First, further work can be performed using a one-dimensional pulse receiver as follows: as physiological motions caused by respiratory and cardiac cycles are reproducible, MR imaging can be used in a preceding training step to relate the US speckle pattern to the MR visualised organ displacement. Subsequently, during therapy, the US speckle pattern can be compared in real time with the training data in order to retrieve the corresponding organ position. The main limitation of this approach arises from the fact that no direct displacement measurement is obtained using US, as the correlation between MRI and US measurement is performed with different units. Second, an extension of the method would be to investigate the use of two-dimensional/three-dimensional US information to identify complex target motion in oblique angles with respect to the probe. Pernot *et al.* (6) used four pulse receivers to estimate the three-dimensional displacement of the targeted organ (three transducers were required to estimate the displacement, and another was added to increase the robustness of the process). However, the challenge of such an approach is when US is obstructed by ribs and/or air in the beam path. For the analysis of nonrigid displacements under real-time conditions, an acceleration of image processing will be required.

This is achievable, for example, by offloading all computationally intensive calculations to a dedicated graphics processing unit (18). Nevertheless, the results offer perspectives for the correction of more complex motion patterns in real time. This fast estimation of complex organ deformation may improve the safety of the intervention by increasing the precision of the focal point position adjustment with target displacement, an important factor when high-power amplitudes are used for energy deposition.

### Acknowledgements

Ligue Nationale Contre le Cancer, Conseil Régional d'Aquitaine, Diagnostic Molecular Imaging EC-FP6-project LSHB-CT-2005-512146; Agence National de la Recherche (project 'MRgHIFU-ALKT'); Philips Healthcare.

### REFERENCES

1. Stewart EA, Rabinovici J, Tempany CMC, Inbar Y, Regan L, Gastout B, Hesley G, Kim HS, Hengst S, Gedroye WM. Clinical outcomes of focused ultrasound surgery for the treatment of uterine fibroids. *Fertil Steril.* 2006; 85: 22–29.
2. Furusawa H, Namba K, Thomsen S, Akiyama F, Bendet A, Tanaka C, Yasuda Y, Nakahara H. Magnetic resonance-guided focused ultrasound surgery of breast cancer: reliability and effectiveness. *J Am Coll Surg.* 2006; 203: 54–63.
3. Hindman J. Proton resonance shift of water in the gas and liquid states. *J Chem Phys.* 1966; 44: 4582–4592.
4. Denis de Senneville B, Mougnot C, Moonen CTW. Real time adaptive methods for treatment of mobile organs by MRI controlled high intensity focused ultrasound. *Magn Reson Med.* 2007; 57: 319–330.
5. Mougnot C, Salomir R, Palussière J, Grenier N, Moonen CTW. Automatic spatial and temporal temperature control for MR-guided focused ultrasound using fast 3D MR thermometry and multispiral trajectory of the focal point. *Magn Reson Med.* 2004; 52: 1005–1015.
6. Pernot M, Tanter M, Fink M. 3D real-time motion correction in high intensity focused ultrasound therapy. *Ultrasound Med Biol.* 2004; 30: 1239–1249.
7. Günther M, Feinberg DA. Ultrasound-guided MRI: preliminary results using a motion phantom. *Magn Reson Med.* 2004; 52(1): 27–32.
8. Gavrilov LR, Hand WH. A theoretical assessment of the relative performance of spherical phased arrays for ultrasound surgery. *IEEE Trans Ultrason.* 2000; 47: 125–139.
9. Maintz JBA, Viergever MA. A survey of medical image registration. *Med Image Anal.* 1998; 2: 1–36.
10. Barron JL, Fleet DJ, Beauchemin SS. Performance of optical flow techniques. *Int J Comput Vis.* 1994; 12: 43–77.
11. Schunck BG, Horn KP. Determining optical flow. *Artif Intel.* 1981; 17: 185–203.
12. de Zwart JA, Vimeux F, Palussière J, Salomir R, Quesson B, Delalande C, Moonen CTW. On-line correction and visualization of motion during MRI-controlled hyperthermia. *Magn Reson Med.* 2001; 45: 128–137.
13. Friston KJ, Ashburner J, Frith CD, Poline JB, Heather JD, Frackowiak RSJ. Spatial registration and normalisation of images. *Hum Brain Mapp.* 1995; 2: 165–189.
14. Champeney DC. *Fourier Transforms and Their Physical Applications.* Academic Press: London, 1973; 68–71<sup>Q8</sup>.
15. Kuglin CD, Hines DC. The phase correlation image alignment method. *Proceedings of the International Conference on Cybernetics and Society* 1975; 163–165<sup>Q9</sup>.
16. Vigen KK, Daniel BL, Pauly JM, Butts K. Triggered, navigated, multi-baseline method for proton resonance frequency temperature mapping with respiratory motion. *Magn Reson Med.* 2003; 50(5): 1003–1010.
17. Dragonu I, Denis de Senneville B, Quesson B, Moonen CTW, Ries M. Real-time geometric distortion correction for interventional imaging with EPI. *Magn Reson Med.* 2008; 61(4): 994–1000.
18. NVIDIA Corporation. *NVIDIA CUDA: Compute Unified Device Architecture, Programming Guide, 2.0 edn.* Publisher: Town, 2008; 1–107<sup>Q10</sup>.

61  
62  
63  
64  
65  
66  
67  
68  
69  
70  
71  
72  
73  
74  
75  
76  
77  
78  
79  
80  
81  
82  
83  
84  
85  
86  
87  
88  
89  
90  
91  
92  
93  
94  
95  
96  
97  
98  
99  
100  
101  
102  
103  
104  
105  
106  
107  
108  
109  
110  
111  
112  
113  
114  
115  
116  
117  
118  
119  
120